JOURNAL OF Materials CHEMISTRY

The physical and chemical properties of electroless nickel–phosphorus alloys and low reflectance nickel–phosphorus black surfaces

Richard J. C. Brown,* Paul J. Brewer† and Martin J. T. Milton

Analytical Science Group, National Physical Laboratory, Teddington, Middlesex, UK TW11 0LW. E-mail: richard.brown@npl.co.uk; Fax: +44 (0)20 8943 6755; Tel: +44 (0)20 8953 6409

Received 9th May 2002, Accepted 18th June 2002
First published as an Advance Article on the web 30th July 2002

Novel insights into the manufacture of nickel–phosphorus black surfaces by chemical etching of electroless-deposited Ni–P alloy has been achieved by examining the influence of pre-etch phosphorus composition and etching method on the resulting morphology, composition and reflectance of the black surface produced. An optimum phosphorus composition and etching regime to produce low reflectance blacks of 0.4% or lower in the visible region is proposed. Cross-sectional analysis of the etched surface has allowed, for the first time, an accurate determination of the scale of the enhanced morphologies produced and the thickness of the oxidised black layer itself. AFM studies have also provided information on the phase structure of the as-deposited Ni–P alloy.

1 Introduction

It has been known for over two hundred years that mixtures of nickel and phosphorus react vigorously when heated.[1] The electroless deposition of metallic nickel in the presence of hypophosphite in aqueous solution was first noted by Wurtz in 1844,[2] but it was not until the accidental re-discovery of the technique by Brenner and Riddell in 1946[3–5] that the reaction was developed on an industrial scale. Further research by Gutzeit in the 1950s led to the scientific basis of most modern electroless nickel plating technologies.[6] The excellent wear and corrosion resistance properties of the coatings have seen the electroless nickel industry expand enormously in recent years. The presence of hypophosphite as a reducing agent in electroless nickel baths ensures the co-deposition of phosphorus,[7–9] usually yielding a mass fraction of phosphorus of 4–12% of the total elemental composition, resulting in the formation of a Ni–P alloy. Electroless nickel deposits containing nickel–boron alloys are also quite common.[10] Composite Ni–P alloys have also been manufactured with such materials as amorphous carbon,[11] diamond[12] and PTFE[13] in order to further enhance their tribological properties.

Ultra-black surfaces are of increasing importance in many fields of science and technology. They are used as very low reflectance coatings in optical instruments and sensors making measurements in the ultra-violet, infrared and visible spectral regions. In particular, they can improve the absorbance of thermal detectors and reduce the effect of stray and scattered light in optical instruments. The latter is of significance when it is necessary to reduce the physical size of instruments whilst not compromising performance. An interesting and little researched property of Ni–P alloys is that they may be chemically treated ('etched') to produce black coatings ('Ni–P black') that can act as very efficient absorbers. Such a procedure usually involves the acid etching of low (1–3% phosphorus) or medium-low nickel–phosphorus (3–6% phosphorus) alloys. Higher phosphorus content alloys are not suitable because they are too corrosion resistant to blacken as a result of acid etching.[14] The main components of the black coating are recognised to include NiO, Ni_2O_3 and some nickel phosphate.[15,16] The first to realise the benefits of this process, a full understanding of which is still lacking, were Kumar *et al.*,[15] who proposed using the coatings for photothermal conversion. Some further work followed, aimed at solar energy applications,[17,18] optical absorbers[19] and a greater understanding of the role of surface morphology in dictating optical characteristics.[20,21]

The process of surface blackening and the relationship of the chemical composition and physical characteristics of the etched surface to the original plating conditions and the etching parameters have never been properly investigated. The experimental work and discussion presented in this paper attempts to extend the current knowledge and theory in these areas and demonstrates that a sounder understanding of the processes involved enables high yield production of Ni–P black surfaces exhibiting a specular reflectance of less than 0.4% at 633 nm. We have been able to quantify the effect of different etching techniques and times and different Ni–P alloy compositions on the surface morphology and the quality of the Ni–P black surface. The use of commercially available substrates and proprietary solutions also represents the first investigation of a process to produce Ni–P black on a large scale.

2 Experimental

Experiments were conducted on two different scales: a 300 l 'industrial scale' bath was used for coating several substrates simultaneously, whilst a laboratory scale preparation, using 1–5 l beakers, was used to plate single samples. Aluminium and copper substrates (40 × 40 × 1 or 120 × 120 × 1 mm plates) were coated. Copper substrates were only coated on the laboratory scale. Plating and preparative solutions (made up with tap water on the industrial scale and distilled water on the laboratory scale) were purchased from MacDermid-Canning, unless otherwise stated. Aluminium substrates (alloy HE30) were initially degreased in a 20% by volume aqueous solution of ALPREP 230 (mostly phosphoric acid and detergent) (80 °C, 15 min), thoroughly rinsed (water) and then placed into

†Present address: Department of Chemistry, Imperial College of Science, Technology and Medicine, London, UK SW7 2AY.

a de-oxidising bath of a 10% by volume aqueous solution of ALPREP 290 (mostly sulfuric acid) (40 °C, 3 min). After further washing in water, the plates had a thin zinc layer applied by immersion in a 25% by volume aqueous solution of ALZINATE (an alkaline zinc preparation) (30 °C, 15 s). Copper substrates (Goodfellow, 99.9%) were prepared by immersion in 0.05% by weight $PdCl_2$ (Aldrich) in 0.1 M HCl (Aldrich) (40 °C, 1 min). These substrates were allowed to dry and then immersed in a smaller Ni–P plating bath (5 min) before being transferred to the main plating bath. For both types of substrate, the same plating bath composition was used: 5% by volume NIKLAD A (mostly nickel sulfate) and 15% by volume NIKLAD B (mostly sodium hypophosphite). Bath loadings were kept between 14 and 32 $cm^2 l^{-1}$. The plates were immersed for 5 h at 88 °C.

After plating, etching was carried out using four different methods. Method 1: immersion in a solution containing 6.0 M sulfuric acid (Aldrich) and 4.0 M nitric acid (Aldrich) (60 °C, 20 s). Method 2: immersion in 9.0 M nitric acid (40 °C, 40 s). Method 3: immersion in a solution containing 5.5 M sulfuric acid and 4.1 M sodium nitrate (Aldrich) (50 °C, 40 s). Method 4: Method 1 followed by rinsing and drying of the artefact, followed by Method 2.

All four methods were followed by thorough rinsing of the artefacts. Methods 1 and 4 are novel. Methods 2 and 3 are included for comparison and are adapted from previous publications.[19,20]

Investigation of the Ni–P and Ni–P black coating microstructure and chemical compositional analysis was carried out with a Camscan Series-2 SEM which was fitted with a Link AN10000 EDX system. An accelerating voltage of 20 kV was used. Secondary electron images of the coated surfaces were obtained at sample angles of 0 (flat) and 45° (tilted). For quantitative chemical microanalysis, EDX spectra were obtained from four randomly selected areas on the coated surfaces of each sample at the same accelerating voltage with 100 s live time and 35 mm working distance. These spectra showed the presence of Ni and P, with a trace of calcium when tap water was used in the plating solution. Oxygen was detected in the "windowless" mode of the EDX detector, but it was not possible to analyse it quantitatively. Elemental compositions were obtained by automatic processing of the EDX spectra using the Link ZAF-4/FLS program. The AFM images were created using a Park Autoprobe CP AFM in intermittent contact mode using ultralever tips with nominal spring constants of 25 N m^{-1}. Visible reflectance measurements on the Ni–P samples were carried out using a 300 mm diameter integrating sphere and a 30 mW He–Ne laser operating at 633 nm.

3 Results and discussion

We commence the discussion by presenting the measured optical properties of the etched surfaces. We then go on to show how these can be understood through an analysis of the detailed properties of the surface. All alloy compositions are given in terms of w, defined as

$$w = \frac{\text{mass of phosphorus}}{\text{mass of all elements}}$$

and are expressed as a percentage.

3.1 Effect of phosphorus content on the produced Ni–P black

The phosphorus content and structure of the plated electroless nickel are known to have a great influence on both the chemical[10,22,23] and electrochemical[24–27] *anti*-corrosion and *anti*-wear properties of the plated alloy. In general, the greater the P content, the more resistant the surface to acid etching. We have found that none of the etching methods employed could etch alloys containing more than 14% P. This is consistent with a general finding that the lower the initial P content of the Ni–P alloy, the greater the extent of the etching and the lower the reflectance of the resulting surface. This relationship is displayed in Fig. 1.

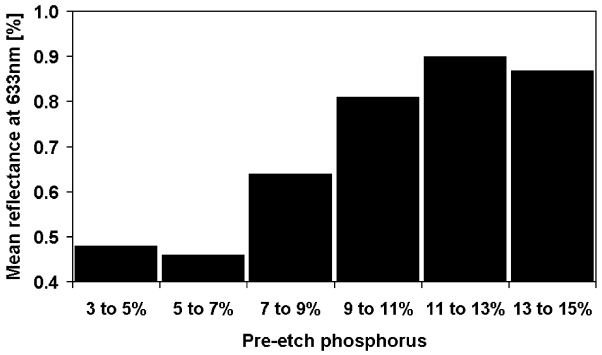

Fig. 1 The average reflectance at 633 nm of Ni–P blacks with varying nominal pre-etch phosphorus compositions.

Fig. 1 shows that, in general, the Ni–P blacks exhibiting the lowest reflectance had the lowest pre-etch P content (with a minimum mean reflectance at 5 to 7%). We propose that as the P content increases, the reflectance increases, because etching is less complete. This is because of the higher chemical resistance which leads to a macroscopically less black material and, additionally, a surface with less developed microscopic morphological properties. Since reflectance measurements carried out on a polished nickel oxide disc yielded values of several percent, it is clear that morphology plays the crucial role in producing the low reflectance of these surfaces. On the laboratory scale, where there is less variation in the quality of the Ni–P plated alloy, we have routinely and regularly produced Ni–P blacks averaging 0.4% reflectance (at 633 nm).

The difference in the morphology of the blackened surface from high and low phosphorus content alloys can be clearly seen by SEM (Fig. 2). Fig. 2(a) is typical of Ni–P alloys with

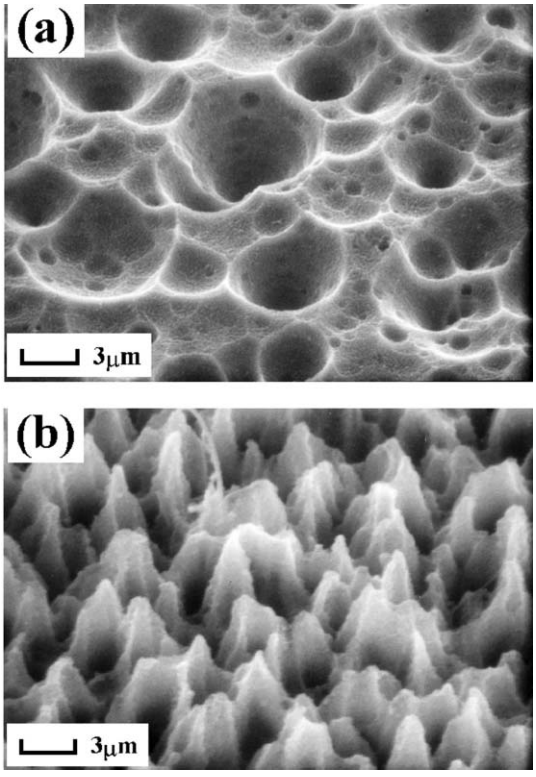

Fig. 2 SEM images (45° elevation) of Ni–P blacks with pre-etch phosphorus compositions of 5–7% (a) and 11–13% (b).

phosphorus contents up to approximately 8%, which produce a very pronounced 'crater' morphology. Alloys with a P content over 8% produce a 'stalagmite-like' morphology [Fig. 2(b)]. The imprecise boundary between the two regimes demonstrates the inherent variability in both the chemical plating and etching processes. Such variability is a much more serious consideration when plating on an industrial scale, since additional factors such as the plate position in the bath, stirring efficiency and temperature distribution are of importance. We have noted that alloys produced on the industrial scale, even after fractional bath turnovers, can produce a range of reflectance values, even with approximately the same P content (as measured by EDX). We propose that such variability is due to differences in the structure of the as-plated Ni–P alloy. The presence of reaction products in the bath, the depletion of the active plating chemicals and changes in the effective bath loading are all thought to contribute to this phenomenon.

It has been observed that as the phosphorus content of the alloy increases, the crater/stalagmite-like features decrease in size and separation. Again, this is thought to be a function of the structural composition of the film. The variation in the scale of the morphological features after etching with initial phosphorus content is shown in Fig. 3. Clearly, the alloy with the higher initial phosphorus content shows smaller etched features and smaller separations between the features.

Substantial work on the calculation of the Ni–P phase diagram[11,28–30] suggests that equilibrium phase Ni–P alloys with up to 15% P consist entirely of the crystalline Ni_3P phase. However, it is known[31] that electrodeposition, chemical bath deposition, vapour deposition and sputtering all produce amorphous or metastable Ni–P phases that do not exist within the standard phase diagram. Such 'non-equilibrium' phases may transform into 'equilibrium phases' under certain conditions, for instance, a catalytic effect caused by impurities.[32] Although this is not thought to be a consideration here, it may limit the usefulness of these unstable phases in sensitive long lifetime applications.[33] Above about 12% P, chemically deposited Ni–P films are amorphous,[34] but in the range under study here, below about 12% P, there are metastable solid solutions within which high phosphorus species such as Ni_3P or Ni_5P_2 exist extensively, or as inclusions in low P content alloys. Such inclusions can manifest themselves in extreme cases as shiny unetchable pinholes on the Ni–P alloy. This has also been observed extensively, particularly when bath agitation was insufficient.[10]

X-Ray diffraction data throughout the literature[22,34–37] show that in both microcrystalline and amorphous deposits, there are numerous precipitated inclusions. Furthermore, it has been shown in the literature[22] that within the compositions of electroless Ni–P alloy that have been produced in this study, glassy nickel phases are observed, with minor constituents of microcrystalline nickel, Ni_5P_2 and Ni_3P (and even some $Ni_{12}P_5$). It has also been observed that Ni–P alloys with between 7–10% P exhibit both microcrystalline and amorphous regions, which may result from a metastable thermodynamic equilibrium between these two regions. Problems associated with X-ray measurements to determine crystallite size have been dealt with in some detail.[38] The X-ray diffraction patterns of electroless Ni–P gradually change from sharp peaks to very broad peaks with increasing P content, as the structural composition slowly evolves from crystalline to amorphous. For crystalline substances, the discrete interference lines become wider as the crystallite size gets smaller,[35] so with crystallites below about 200 nm in size, the distinction between an alloy being finely crystalline and amorphous is ambiguous.

Fig. 4 shows an X-ray diffractogram of an as-plated Ni–P alloy produced in this study on the 'industrial scale'. The two broad, coalescing peaks centred around $2\theta = 47^\circ$ and the smaller hump at $2\theta = 25^\circ$ are totally consistent with an alloy of glassy composition exhibiting short to medium range order with embedded crystalline precipitates.

We propose that as the Ni–P alloys being produced are metastable solid solutions, the morphology of the Ni–P black after etching is due to the relative amounts of high phosphorus inclusions within the alloys. Ni–P alloys with a lower P content are etched more completely, with large crater formation as large portions of the alloy are dissolved, whilst as the P content increases, it is more difficult for large swathes of Ni–P to be etched and we observe narrower, sharper features. The two prevalent morphologies may be considered to be closely related. With low phosphorus alloys, for a given unit volume, more Ni–P is etched away than is unetched, giving large craters and thin, short stalagmites, whereas, for high phosphorus alloys, less Ni–P is etched away than is left and the result is larger, broader stalagmites and thinner craters. There is evidence to support this theory since, if the elemental content of the alloys after an initial short etch is examined, the P content of the surface layer is found to be much higher, suggesting that the nickel is preferentially removed.

AFM images of the pre-etched alloys support the view that the overall composition of the Ni–P films is that of an

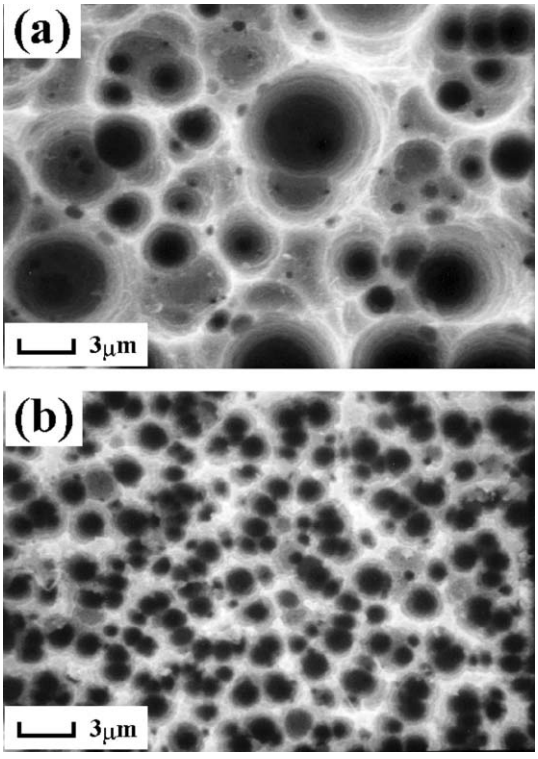

Fig. 3 SEM images (top view) of Ni–P blacks with pre-etch phosphorus compositions of 5–7% (a) and 9–11% (b).

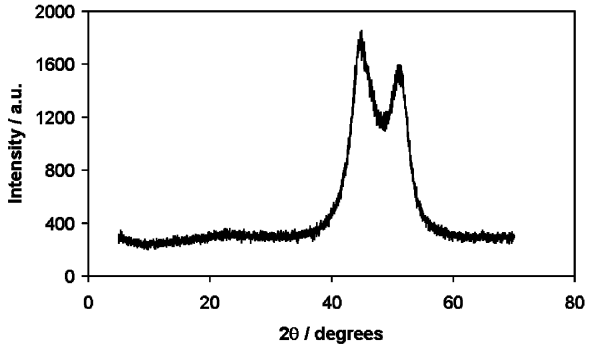

Fig. 4 X-Ray diffractogram of an as-plated Ni–P alloy produced on the industrial scale.

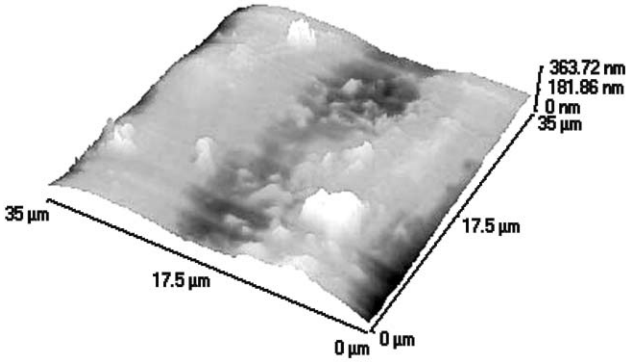

Fig. 5 AFM image of an as-plated Ni–P surface before etching, showing inclusions within the Ni–P alloy.

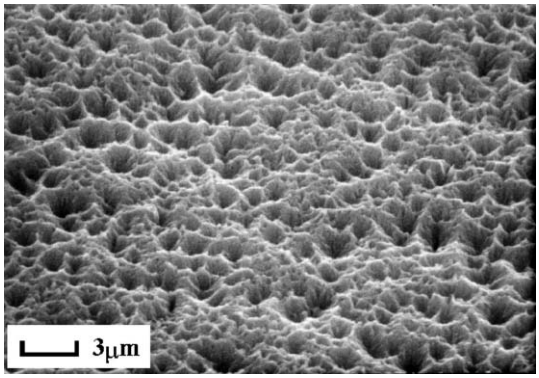

Fig. 6 SEM image (45° elevation) of a Ni–P surface having undergone etching by Method 1.

amorphous and crystalline composite. An image demonstrating this is shown in Fig. 5. The majority of the image shows a relatively flat surface with gradual changes in topography. This is proposed to represent the part of the Ni–P film showing a glassy composition. On the flat surface are several raised features and some depressed features. Such inclusions have been proposed previously.[39] The transition from the flat glassy Ni–P to these features is sharp and multilayer steps with very short terraces can be observed on moving across the surface. The geometric stepped shapes of these features provide further evidence for the presence of crystalline character within the film and these areas are believed to represent crystalline inclusions within the Ni–P film exhibiting higher phosphorus content (probably Ni_5P_2 and Ni_3P) than the surrounding composition. Furthermore, it is proposed that etching is initiated preferentially at these boundaries between crystalline and amorphous phases and at the edge of crystalline terraces owing to the higher Gibbs free energy at these sites. In this way, the number, size and separation of these crystalline inclusions, which is related to P content within the Ni–P alloy, will dictate where etching occurs most vigorously and most extensively. This, in turn, will dictate the eventual morphology of the etched alloy and its reflection characteristics.

3.2 The effect of etching technique on mass loss from the plated surface

Mass loss data acquired after Ni–P plating, and after the first and second etching steps is useful in indicating the vigour of each etching regime and the extent to which each process affects the Ni–P alloy. In this way, the most effective etching regime can be determined and unnecessary steps may be eliminated. A slight gross gain in mass will occur at the interface during the etching process due to the production of the oxidised alloy at the surface of the Ni–P black layer. This mass gain is negligible in relation to the total loss from alloy dissolution and the mass data can therefore be considered simply in terms of the dissolution process. Table 1 shows the recorded mass of three plates after electroless nickel plating and during and after the two-stage etching process (Method 4). The data show that the first etching stage removes approximately 25% of the electroless nickel coating. Plate E, however, shows a much lower reduction in mass. As the plates were produced at the same time in the industrial size electroless nickel bath, it is possible, due to location, that this plate had a larger phosphorus content and therefore the etching process was slower. A smaller mass loss is shown for the second etching process, indicating a more chemically selective process and a less harsh etching solution. In this case, the mass loss for plate E is much closer to the other plates. Therefore, if the phosphorus content is higher in this plate, this provides further evidence concerning the less chemically selective nature of the second etch. Mass loss values show that, on average, approximately half of the electroless nickel alloy is lost during the two-stage etching process (Method 4).

3.3 The effect of etching method on morphology and reflectance

Fig. 6 shows a surface, etched using Method 1, consisting of shallow features indicative of mild penetration into the substrate surface. Owing to the preferential reaction of the acidic solution with nickel-rich areas in the alloy, as opposed to phosphorus inclusions, Method 1 produces a chemically selective etch resulting in higher residual surface phosphorus contents after etching. This demonstrates that Method 1 produces only very minor morphological enhancement, and has resulted in the use of the other three etching methods for the production of black surfaces.

Data retrieved from EDX measurements taken on three alloys using the two-stage etch (Method 4) are shown in Table 2. The first etching stage results in a large increase in the phosphorus content from preferential dissolution of the nickel. The phosphorus content then reduces after the second etch to a composition similar to the original alloy. This indicates the less selective nature of the second etch. This results in more extensive etching and a deeper morphology. The deep crater formation is responsible for the visibly blacker surface in comparison to the shiny appearance of the alloy after the first process. In many cases, the second etch is much slower in the two-stage process than when it is conducted on its own. This may be because the first stage preferentially removes the nickel atoms at the surface; the second etching stage will become more difficult to initiate as the alloy surface now effectively has a high phosphorus content. In some cases, the second stage did not even initiate, which is the reason for the data exclusions in Table 2 for plates B and C. Hence, the first stage of the

Table 1 Mass and reflectance data for five Ni–P coated aluminium substrates undergoing the two-stage etching process (Method 4)

Plate	Post plating mass/g	Plated mass/g	Post 1st etch mass/g	Mass loss (%)	Post 2nd etch mass/g	Mass loss (%)	Reflectance (%)
A	7.12	2.79	6.42	9.8	6.09	5.1	1.07
B	6.68	2.58	6.03	9.8	—	—	—
C	6.36	2.26	5.77	9.4	—	—	—
D	6.48	2.33	5.81	10.4	5.26	9.4	0.55
E	6.32	2.19	6.10	3.4	5.74	6.0	0.97

Table 2 Pre- and post-etch phosphorus compositions and reflectance data for five Ni–P coated aluminium substrates after undergoing the two-stage etching process (Method 4)

Plate	Pre 1st etch P content/wt%	Post 1st etch P content/wt%	Post 2nd etch P content/wt%	Reflectance (%)
A	5.7	16.0	7.4	1.07
B	6.6	18.6	—	—
C	8.2	14.2	—	—
D	8.0	19.0	10.6	0.55
E	8.9	17.1	11.0	0.97

Method 4 process was determined to be unnecessary and it was concluded that the nitric acid etch unaccompanied by the first process was suitable for the production of low reflectance surfaces. This conclusion ruled out Methods 4 and 1 for the effective, reproducible etching of the Ni–P alloys. Methods 2 and 3 proved equally suitable for the production of Ni–P blacks. Despite the use of similar etching techniques in previous studies, the morphology of the etched alloys in this study is not always consistent with the observed morphology from other studies.[19,21]

Etching methods 2 and 3 produced similar reflectance values and morphologies. Method 3, used in a previous study,[19] led to crater formation similar to that observed previously with the other etching methods. However, the crater walls and edges exhibit a jagged appearance. The size of the craters is reduced, with a greater occurrence of pores. This might suggest a more effective structure for producing a low reflectance surface. However, the reflectance values indicate a close comparison to the previous etching methods. This effect may be explained by the depth of the craters. In both cases, the pore depths are of similar size, resulting in Ni–P blacks exhibiting similar reflectances.

3.4 Depth of the etched features and thickness of the Ni–P black coating and consequences for the IR reflectance

Prior to this work, the depth of the pores had only been estimated from elevation SEM views of the etched surface.[20] We believe that this is the first publication of cross-sectional studies of etched Ni–P substrates to determine the pore depth and surface oxide thickness. These are extremely important properties of the surface that define the absorption (and emission) characteristics of electromagnetic radiation.[40] The thickness of the black layer in particular severely limits the reflectance of the surface in the infrared. The smallest thickness of a 90% broad-band dielectric absorber is known to be approximately 1/17 of the longest operating wavelength.[40] Black anodised aluminium alloys are known to be superior absorbers in the far infrared.[41] Cross-sections of a few samples on copper and zincated aluminium substrates were prepared using a standard metallographic procedure in order to assess coating thickness by SEM. Magnification corrections were made by imaging a standard grid (approximately 19.7 lines per mm) under SEM conditions identical to those used to examine the surface topography. Some typical SEM images of cross-sections are displayed in Fig. 7.

The variation in the heights of the peaks and troughs on the cross-sectional pictures is due to two effects. Firstly, the innate variability in the physical composition of the film on this scale and the chemical process of etching ensures that etching will not be uniform across the whole film. Additionally, the cross-section of the etched film very rarely passes directly through the extreme top and bottom of each etched feature, more often giving a conic section of the crater or stalagmite morphology. It is reasonable, therefore, to estimate the pore depth from the height difference between the lowest trough and the highest peak across the length of the cross-sections. For the aluminium substrate, this depth is 11 μm, whilst for the copper substrate, it

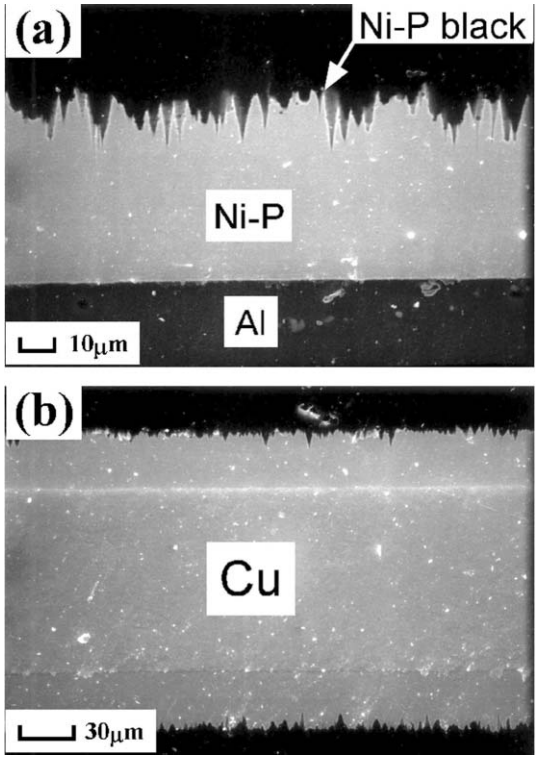

Fig. 7 Cross-sectional SEM images of etched Ni–P layers on aluminium (a) and on both sides of a thin copper substrate (b).

is 10 μm. There is no significant difference between these results within the estimated uncertainty of the measurements, which is as expected, since neither etch is influenced by the substrate. Additionally, the thickness of the entire post-etch Ni–P layer is approximately 40 μm. This value agrees well with an estimated total pre-etch Ni–P thickness of 80 μm (based on plated mass data and density data for various Ni–P compositions[10]), since we know from gravimetric studies that approximately half of the plated mass is removed during etching.

The Ni–P black layer is observed on the SEM images as the thin, lighter band at the outermost edges of the etched layer. The thickness of this layer is approximately 0.75 μm, with little variation along the surface of the cross-section. Such a thickness is likely to limit the performance of the Ni–P black in the infrared but would not impose any fundamental limitation on surface reflectances of 0.35% or better at 633 nm.[40] The thickness of the Ni–P black layer is limited because further penetration will dissolve the outermost part. A thickness of 0.75 μm is the result of this balance between film penetration and concomitant dissolution as a function of time for the alloys under study here. In this way, we propose that the thickness of the Ni–P black layer is directly related to the porosity of the Ni–P alloy. In order to achieve a more porous alloy, it may be necessary to resort to vastly different plating conditions and alternative plating formulations.

The reflectance of the sample in the infrared has been measured. The total, regular and diffuse components of the reflectance are plotted against wavelength in Fig. 8. As expected, the total reflectance of the surface increases significantly in the far infrared, tending towards a maximum reflectance of approximately 85%, although this is mostly a consequence of the increase in regular reflectance, since the diffuse component tends to zero at longer wavelengths. Consistent with the observation that the smallest thickness of a 90% broad-band dielectric radar absorber is 1/17 of the longest operating wavelength[40] the absorbance of the Ni–P black surface does not fall below this level for incident radiation less than 11 μm, which is consistent with our estimate of the Ni–P black surface layer of 0.75 μm. The surface

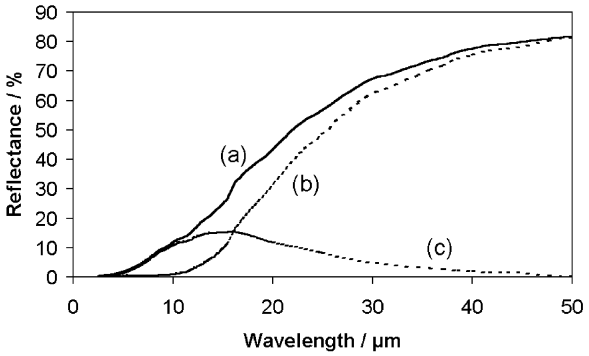

Fig. 8 The total (a), regular (b) and diffuse (c) components of reflectance as a function of wavelength for a Ni–P black surface; measured using a PE580B spectrophotometer fitted with a hemisphere reflectometer.

performs even better at lower wavelengths—the total reflectance not exceeding 1% for wavelengths less than 4.5 μm and the regular component remaining below 1% reflectance for wavelengths less than 10 μm.

4 Conclusions

Ni–P alloys were plated on copper and aluminium substrates on both industrial and laboratory scales. These alloys were then etched in a variety of chemical regimes to produce oxidised Ni–P black surfaces. Using AFM, SEM, elemental analysis and reflectance measurement, conclusions have been drawn about the relationship between as-plated phosphorus content, Ni–P phase structure, post-etch morphology and the reflectance characteristics of the Ni–P blacks.

We conclude that the nickel–phosphorus blacks with the lowest reflectance in the visible region are those with the lowest pre-etch phosphorus composition. SEM images show that alloys low in phosphorus produce a 'cratered' morphology upon etching, whilst those with higher phosphorus contents exhibit 'stalagmite-like' features. This effect is ascribed to the greater chemical resistance to the etch of the high phosphorus content alloys. In addition, as the phosphorus content of a Ni–P alloy increases, the morphological features after etching appear to be smaller and less widely spaced. This is partly attributed to the increased density of high phosphorus inclusions (which are known to be present at these alloy compositions) within the higher phosphorus alloys. Half the plated mass is lost during etching procedures and, whilst there is more variability in the structure and content of alloys produced on the industrial scale, an appropriately chosen etching regime produced low reflectance black surfaces of 0.4% or less in the visible region. Cross-sectional analysis of the etched substrates shows a peak to trough height of about 10 μm, with the top layer of Ni–P black 'oxide' being only 0.75 μm. The thickness of the black top surface is thought to limit the surface's absorption capability in the infrared region, which is born out by reflectance measurements in the far IR.

Acknowledgements

The authors are grateful to Dr Peter Gillespie for useful discussions and to Dipak Gohil for the SEM and EDX data, Dr James Johnstone and Lizzie Inglessi for the AFM images, Mike Smart for the IR reflectance measurements and Peter Haycocks and William Servantes for the visible reflectance measurements.

References

1 M. Pelletier, *Ann. Chim.*, 1792, **13**, 113.
2 A. Wurtz, *C. R. Hebd. Seances Acad. Sci.*, 1844, **18**, 702.
3 A. Brenner and G. E. Riddell, *J. Res. Natl. Bur. Stand. (U. S.)*, 1946, **37**, 91.
4 A. Brenner and G. E. Riddell, *J. Res. Natl. Bur. Stand. (U. S.)*, 1947, **39**, 385.
5 A. Brenner, D. E. Couch and E. K. Williams, *J. Res. Natl. Inst. Stand. Technol.*, 1950, **44**, 109.
6 G. Gutzeit, *Plating*, 1959, **46**, 1158.
7 S. John, N. V. Shanmugham and B. A. Shenoi, *Met. Finish.*, 1982, **80**, 47.
8 L. M. Abrantes and J. P. Correia, *J. Electrochem. Soc.*, 1994, **141**, 2356.
9 K. Parker, *Plat. Surf. Finish.*, 1987, **74**, 60.
10 W. Riedel, *Electroless Nickel Plating*, Finishing Publications Ltd., Stevenage, 1991.
11 L. M. Yupko, A. A. Svirid and S. V. Muchnik, *Sov. Powder Metall. Met. Ceram. (Engl. Transl.)*, 1986, **25**, 763.
12 V. V. N. Reddy, B. Ramamoorthy and P. Kesavan Nair, *Wear*, 2000, **239**, 111.
13 X. Hu, C. Dai and J. Li, *Plat. Surf. Finish.*, 1997, **84**, 51.
14 P. Gillespie, in *Surface Engineering Casebook: Solutions to Corrosion and Wear-Related Failure*, ed. J. S. Burnell-Gray and P. K. Datta, Abingdon Publishing Ltd., 1996.
15 S. N. Kumar, L. K. Malhotra and K. L. Chopra, *Sol. Energy Mater.*, 1980, **3**, 519.
16 M. Wierzbicka and A. Malecki, *J. Therm. Anal. Calorim.*, 1999, **55**, 981.
17 S. John, N. V. Shanmugan, K. N. Srinivasan, M. Selvam and B. A. Shenoi, *Surf. Technol.*, 1983, **20**, 331.
18 K. N. Srivivasan, N. V. Shanmugan, M. Selvam, S. John and B. A. Shenoi, *Energy Convers. Manage.*, 1984, **24**, 255.
19 S. Kodama, M. Horiuchi, T. Kunii and K. Kuroda, *IEEE Trans. Instrum. Meas.*, 1990, **39**, 230.
20 C. E. Johnson, *Met. Finish.*, 1980, **78**, 21.
21 S. Abis and M. C. Baudino, *Mater. Sci. Eng.*, 1986, **77**, L1.
22 R. C. Agarwala and S. Ray, *Z. Metallkd.*, 1988, **79**, 472.
23 W. Ding, M. Wang, C. Hsiao, Y. Xu and Z. Tian, *Scr. Metall.*, 1987, **21**, 1685.
24 S. W. Court, B. D. Barker and F. C. Walsh, *Trans. Inst. Met. Finish.*, 2000, **78**, 157.
25 C. Kerr, D. Barker and F. C. Walsh, *Trans. Inst. Met. Finish.*, 1996, **74**, 214.
26 B. Barker, S. Campbell and F. Walsh, *Trans. Inst. Met. Finish.*, 1997, **75**, B110.
27 C. Kerr, D. Barker and F. Walsh, *Trans. Inst. Met. Finish.*, 1997, **75**, 81.
28 H. Okamoto, *J. Phase Equilib.*, 2000, **21**, 210.
29 J. Koeneman and A. G. Metcalfe, *Trans. Metall. Soc. AIME*, 1958, **212**, 571.
30 J. Shim, H. Chung and D. Lee, *J. Alloys Compd.*, 1999, **282**, 175.
31 K. J. Lee and P. Nash, *Phase Diagrams of Binary Nickel Alloys*, ASTM International, Materials Park, 1991.
32 B. G. Bagley and D. Turnbull, *Acta Metall.*, 1970, **18**, 857.
33 H. Davies, NPL Materials Centre, NPL, Teddington, UK, private communication.
34 S. V. S. Tyagi, V. K. Tandon and S. Ray, *Z. Metallkd.*, 1985, **76**, 492.
35 K. Itoh, F. Wang and T. Watanabe, *J. Japan Inst. Met., Sendai*, 2001, **65**, 495.
36 H. Yamasaki, H. Izumi and H. Sunada, *Scr. Metall.*, 1981, **15**, 177.
37 R. M. Allen and J. B. Van der Sande, *Scr. Metall.*, 1982, **16**, 1161.
38 H. Kreye, H. Muller and T. Petzel, *Galvanotechnik*, 1986, **77**, 561.
39 R. J. Keyse and C. Hammond, *Mater. Sci. Technol.*, 1987, **3**, 963.
40 K. N. Rozanov, *IEEE Trans. Antennas Propag.*, 2000, **48**, 1230.
41 T. Shelley, *Eureka*, 2001, **21**, 39.